Interdisciplinary Sciences: Computational Life Sciences (2018) 10:311–319
https://doi.org/10.1007/s12539-017-0278-8

ORIGINAL RESEARCH ARTICLE

# Detoxification of aflatoxins on prospective approach: effect on structural, mechanical, and optical properties under pressures

**Yong-Kai Wei[1] · Xiao-Miao Zhao[2] · Meng-Meng Li[2] · Jing-Xin Yu[1] · Selvaraj Gurudeeban[2] · Yan-Fei Hu[3] · Guang-Fu Ji[4] · Dong-Qing Wei[2,5,6]**

Received: 6 November 2017 / Revised: 6 December 2017 / Accepted: 12 December 2017 / Published online: 27 December 2017


**Abstract**
Aflatoxins are sequential of derivatives of coumarin and dihydrofuran with similar chemical structures and well-known carcinogenic agent. Many studies performed to detoxify aflatoxins, but the result is not ideal. Therefore, we studied structural, infrared spectrum, mechanical, and optical properties of these compounds in the aim of perspective physics. Mulliken charge distributions and infrared spectral analysis performed to understand the structural difference between the basic types of aflatoxins. In addition, the effect of pressure, different polarized, and incident directions on their structural changes was determined. It is found that $AFB_1$ is most stable structure among four basic types aflatoxins ($AFB_1$, $AFB_2$, $AFG_1$, and $AFG_2$), and IR spectra are analyzed to exhibit the difference on structures of them. The mechanical properties of $AFB_1$ indicate that the structure of this toxin can be easily changed by pressure. The real $(\varepsilon_1(\omega))$ and imaginary $(\varepsilon_2(\omega))$ parts of the dielectric function, and the absorption coefficient $\alpha(\omega)$ and energy loss spectrum $L(\omega)$ were also obtained under different polarized and incident directions. Furthermore, biological experiments needed to support the toxic level of $AFB_1$ using optical technologies.

**Keywords** Aflatoxins · Mulliken charge distributions · Infrared spectrums · Mechanical properties · Optical properties

## 1 Introduction

Aflatoxins are sequential of derivatives of coumarin and dihydrofuran with similar chemical structures and well-known carcinogenic agent. As the secondary metabolites of Aspergillus flavus and Aspergillus parasiticus [1, 2], above 20 different types of aflatoxins have been isolated and identified, among which $AFB_1$, $AFB_2$, $AFG_1$, and $AFG_2$ are four basic types. Aflatoxins occur in many countries, especially in the tropical and subtropical regions where the conditions of temperature and humidity are optimal for the growth of moulds and for the production of the toxin. Agriculutral commodities and important crops are susceptible to such contamination. Aflatoxin contamination is considerable serious in the progress of crop receipt, storage, and transportation [3–7]. The removing of aflatoxins in foods and feed with high efficient and safe method is a significant subject in the field of agriculture and industry of grain and oil.

In general, aflatoxins are insoluble in water, petroleum ether, ethyl ether, and ethane, but dissolved in polar solvents such as methanol, acetone, and chloroform. Furthermore, aflatoxins are relatively stable in neutral solution and can be slightly decomposed in strong acidic solution. Aflatoxin

✉ Yan-Fei Hu
lsdwrk@163.com

✉ Dong-Qing Wei
hngydqwei@sina.com

1 College of Science, Henan University of Technology, Zhengzhou 450001, China

2 Centre of Food Science and Engineering, School of Chemistry, Henan University of Technology, Zhengzhou 450001, China

3 School of Science, Sichuan University of Science and Engineering, Zigong 643000, China

4 National Key Laboratory of Shock Wave and Detonation Physics, Institute of Fluid Physics, Chinese Academy of Engineering Physics, Mianyang 621900, China

5 The State Key Laboratory of Microbial Metabolism, College of Life Science and Biotechnology, Shanhai Jiao Tong University, Shanghai 200240, China

6 State Key Laboratory of Explosion Science and Technology, Beijing Institute of Technology, Beijing 100081, China

$B_1$ ($AFB_1$) is the most toxic, mutagenic, and carcinogenic in nature, classified as level-1carcinogen by the Word Health Organization (WTO). It is most common in naturally contaminated foods [8]. The structure of $AFB_1$ is composed of a two-furan ring (basic toxic structure) and an oxidized naphthalene ortho ketone (carcinogenic structure). In fact, $AFB_1$ is not carcinogenic before metabolic activation. However, $AFB_1$ is translating into strong carcinogenic under the metabolic action of the mixed-functional oxidase in hepatocyte endoplasmic reticulum microsomes after entering body. Thus, $AFB_1$ is also known as pre-carcinogen. A number of physical, chemical, and biological methods employed to change the basic structure of aflatoxins [8–10].

According to the chemical properties of aflatoxin, there are mainly three ways to reduce the toxicity, i.e., physical, chemical, and biological methods [11–15]. Physical methods mainly include high-temperature method [16], ultraviolet irradiation [17], and γ-ray irradiation [18]. High temperature can destroy the aflatoxin molecule and reduce its toxicity, but also degrades the nutritional content of food. This method is not suitable for the removal of aflatoxins in food. Furthermore, UV irradiation is used in the food industry, due to its common disinfecting and sterilizating nature. Because of UV irradiation, aflatoxins could degrade to some extent. However, UV irradiation also not ideal, since the penetration of UV light is weak. Thus, it can work in the surface of material, while cannot be exposed to $AFB_1$ inside [17]. γ-ray is the atomic energy level transition when the radiation releases with strong penetration and high cell lethality. Studies have shown that γ-ray can inhibit the growth of aspergillus flavus and can inactivate aflatoxin [18]. Irradiation can be used for food sterilization and preservation, and also be applied to the removal of pollutants. However, there are still unavoidable problems in the application of irradiation technology in food quality and safety. Due to the different understanding of irradiated food, the degree of recognition and acceptance is limited in the daily life. Some studies indicate radiation could change the quality of food, and the radiation itself acts as pollutant, resulting in strict restriction about the application of radiation technology in the field of food. Montmorillonite can also adsorb aflatoxins and the maximum adsorption capacity was above 600 μg/g, but the adsorption could not completely remove residual toxin in food [11]. The chemical method mainly involves the change the molecular structure of aflatoxins, translating them into non-toxic or low-toxic nature. As chemical treatment can change the color of food and increase the content of non-protein nitrogen, results indicate not suitable method to remove aflatoxins from contaminated food. Biological methods include biological enzymatic hydrolysis, microbial adsorption, as well as degradation of toxins by microbial metabolites, whereas the toxin also cannot remove thoroughly [10].

Based on the literature information, the detoxification of aflatoxins still cannot be resolved yet. Therefore, it is need to explore new and efficient detoxification methods. The ideal method of detoxification requires: (1) high toxicity, toxin is destroyed or converted into non-toxic compounds; (2) low price, easy to implement; (3) does not produce toxic products and does not affect the physical quality or chemical quality. Using pressure can efficiently transform the properties of the toxic substances[9]. In addition, AFB1 is the most stable structure among different types of aflatoxins. Hence, we made an effort under pressure-dependent changes for structural, mechanical, and optical properties to detoxify aflatoxins.

## 2 Computational details

The basic structure of $AFB_1$ molecule under different temperatures was obtained by Avogadro code [19], and then, infrared spectrum was calculated using Gaussion program combined with B3LYP/6-31G(d) SP basis set [20]. The calculations on mechanical and optical properties performed with the Cambridge Serial Total Energy Package (CASTEP) program [21, 22], using density function theory with Norm-conserving pseudopotentials [23]. The generalized gradient approximation (GGA) with Perdew–Burke–Ernzerhof (PBE) parametrization was employed [24]. The cut-off energy for plane waves was set to 500.0 eV. The pseudoatomic calculations were performed for H $1s^1$, C $2s^2 2p^2$, and O $2s^2 2p^4$. Brillouin-zone sampling was performed using Monkhorst–Pack scheme with a *k*-point grid of $4 \times 4 \times 2$ [25]. The values of the kinetic energy cutoff and the *k*-point grid were determined to ensure the convergence of the total energies to within 0.01%. The structures under pressures were relaxed using Broyden–Fletcher–Goldfarb–Shannon (BFGS) method [26, 27]. In the geometry relaxation, the total energy of the system converged to less than $1.0 \times 10^{-6}$ eV/atom, the residual force to less than 0.002 eV/Å, the displacement of atoms to less than 0.002 Å, and the residual bulk stress to less than 0.1 GPa. The structure of $AFB_1$ was obtained from Cambridge structural database (CSD) operated by CCDC [28], which has been affirmed by experiments under room temperature. Our calculations performed on the one unit cell with four molecules in the geometry optimization. The hydrostatic pressure range of our calculations was 0–70 GPa. The crystal parameters of $AFB_1$ are applied as $a = 7.840$, $b = 6.360$, $c = 28.350$, and the crystal belongs to Orthorhombic (space group: 19, P212121).

## 3 Results and discussion

### 3.1 Basic structures and Infrared (IR) spectra of aflatoxin

The results confirmed that the furan ring is the basic toxic structure and the oxidized naphthalene ortho ketone is the carcinogenic structure in the four basic types of aflatoxin structures ($AFB_1$, $AFB_2$, $AFG_1$, and $AFG_2$). The detoxification of aflatoxin is corresponding to the destruction of furan ring and oxidized naphthalene ortho ketone in the structure of aflatoxin. It is necessary to have a deep understanding on the basic molecular structures and the difference among four basic structures of aflatoxin. The basic molecular structures of $AFB_1$ ($C_{17}H_{12}O_6$), $AFB_2$ ($C_{17}H_{14}O_6$), $AFG_1$ ($C_{17}H_{12}O_7$) and $AFG_2$ ($C_{17}H_{14}O_7$) combined with Mulliken atomic charge distribution are illustrated in Fig. 1. The basic toxic structure (two-furan ring structure) and carcinogenic structure (oxidized naphthalene ortho ketone) are also marked in each molecule. The red and green colors represent the density of states of electrons, indicating the addition and loss of electrons, respectively. In the two-furan ring structure, the Mulliken charge of O5 atoms in $AFB_1$, $AFB_2$, $AFG_1$, and $AFG_2$ are −0.0.525, −0.528, −0.525, and −0.527, while O6 atoms correspond to −0.455, −0,474, −0.455, and −0.473, respectively. Though the charge difference of these four type structures is less, one can find that the Mulliken charge value of O5 and O6 is same for $AFB_1$ and $AFG_1$, and they are also almost same for $AFB_2$ and $AFG_2$. The most obvious character of the oxidized naphthalene ortho ketone structure is the existence of two oxygen atoms (O1 and O4). However, the values of Mulliken charge of O1 and O4 for these four molecules are discrepant. For O1 atom, they are −0.429, −0.431, −0.427, and −0.420 for $AFB_1$, $AFB_2$, $AFG_1$, and $AFG_2$, respectively. For O4 atom, it is −0.541 for $AFB_1$ and −0.540 for $AFB_2$, while −0.533 for $AFG_1$ and −0.531 for $AFG_2$. One can find that the values become less for $AFG_1$ and $AFG_2$ compared with $AFB_1$ and $AFB_2$. Correspondingly, the value of Mulliken charge increases for the carbon atoms linked these two oxygen atoms (C6 for $AFB_1$ and $AFG_1$ and C8 for $AFB_2$ and $AFG_2$). It was demonstrated that $AFB_1$ is most stable structure for aflatoxin and presents

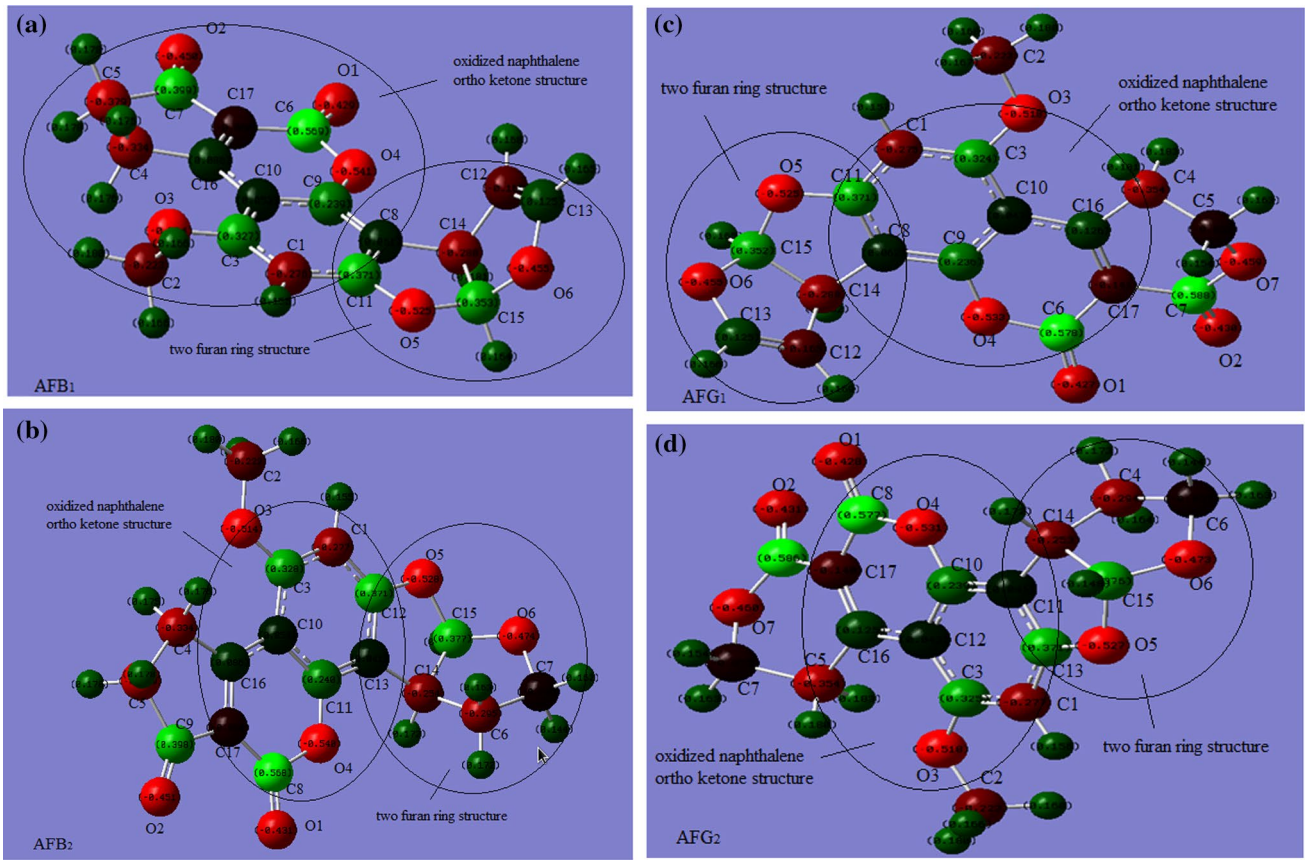


**Fig. 1** Basic molecular structure of **a** $AFB_1$ ($C_{17}H_{12}O_6$), **b** $AFB_2$ ($C_{17}H_{14}O_6$), **c** $AFG_1$ ($C_{17}H_{12}O_7$), and **d** $AFG_2$ ($C_{17}H_{14}O_7$) combined with Mulliken atomic charge distribution. Mulliken charge of C and O atoms is also calculated in each molecule. The basic toxic structure (two-furan-ring structure) and carcinogenic structure (oxidized naphthalene ortho ketone) are also marked in each molecule

the highest toxicity. The bond order between them plays an important role on the stable of these four structures.

Figure 2 shows the IR reflectivity spectra of different aflatoxin structures. The total vibrational modes are 99, 105, 102, and 108 for $AFB_1$, $AFB_2$, $AFG_1$, and $AFG_2$, respectively. Here, the main vibrational modes are given to analyze the obvious change of modes among these four structures. The following spectral changes exist among them: the position of $v_1$ mode in $AFB_1$ and $AFG_1$ is 1883 $cm^{-1}$, but shifts to lower frequency (1876 $cm^{-1}$) for $AFB_2$ and $AFG_2$; the intensity of $v_1$ mode for $AFG_1$ structure corresponds to strongest peak in these four structures. Through the analysis of vibrational modes, $v_1$ mode represents the stretching vibration between C1 and O6 in the oxidized naphthalene ortho ketone structure for both $AFB_1$ and $AFG_1$, indicating that these two bonds are strongest in these four structures. Inversely, it is weakest for the bond formed between C8 atom and O1 atom in $AFB_2$. Another striking difference is the high intensity of $v_3$ mode in $AFB_2$, mainly attributes to the carbon atoms' stretching vibration in the oxidized naphthalene ortho ketone structure, i.e., the vibrations among C1, C3, and C10–C13 carbon atoms. $v_9$ mode mainly results from the vibrations in the furan ring structures, while $v_{10}$ and $v_{11}$ stem from the stretching vibration of hydrogen atoms in methyl groups.

## 3.2 Elastic and mechanical properties

The elastic constants, since the elastic constants of materials under pressure are essential to predict and understand material response, strength, mechanical stability, and phase transition [29]. In general, the number of properties can be calculated from elastic constants [30]. In this work, we mainly studied the mechanical properties of $AFB_1$, since it

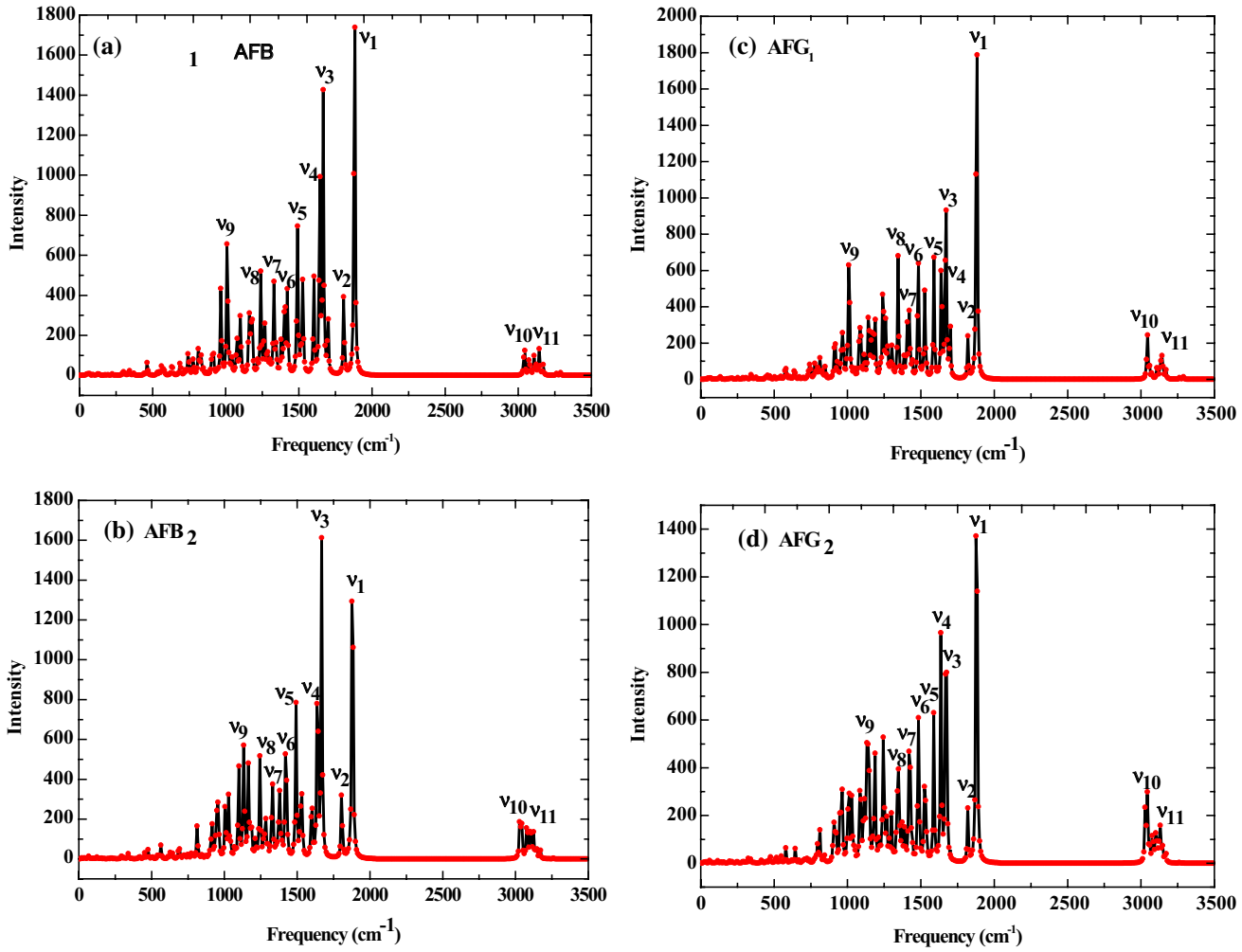


**Fig. 2** Infrared spectra under room temperature of four basic types aflatoxin: **a** $AFB_1$, **b** $AFB_2$, **c** $AFG_1$, and **d** $AFG_2$. The positions of each peaks are indicated with red dots. The main peaks correspond to various vibrational modes are also marked for comparison among these four type structures

is usually found in the greatest concentration in foods and is the most acutely toxic of the aflatoxins. To calculate the elastic constants under hydrostatic pressure, the symmetry-dependent strains are non-volume conserving. The elastic constants, $C_{ijkl}$, with respect to the finite strain variables are defined as follows [29, 31]:

$$C_{ijkl} = \left(\frac{\partial \sigma_{ij}(x)}{\partial e_{kl}}\right)_X. \tag{1}$$

Here, $\sigma_{ij}$ and $e_{kl}$ are the applied stress and Eulerian strain tensors, and $X$ and $x$ are the coordinates before and after deformation, respectively. Under hydrostatic pressure,

$$C_{ijkl} = c_{ijkl} + \frac{P}{2}(2\delta_{ij}\delta_{kl} - \delta_{il}\delta_{jk} - \delta_{ik}\delta_{jl}), \tag{2}$$

where $C_{ijkl}$ denotes the second-order derivatives with respect to the infinitesimal train and $\delta$ is the finite strain variable. The fourth-rank tensor $C_{ijkl}$ generally reduces greatly when taking into account the symmetry of the crystal. In this study, the crystal of $AFB_1$ contains four molecules and belongs to tetragonal structure, and then, $C_{ijkl}$ is reduced to eight components, i.e., $C_{11}$, $C_{22}$, $C_{33}$,$C_{44}$, $C_{55}$, $C_{66}$, $C_{12}$, $C_{13}$, and $C_{23}$. The calculated elastic constants of $C_{ijkl}$ under pressures are given in Fig. 3a. The criteria for mechanical stability are as follows:

$$\begin{aligned}
&C_{11} > 0,\ C_{22} > 0,\ C_{33} > 0,\ C_{44} > 0,\ C_{55} > 0,\ C_{66} > 0,\\
&\left[C_{11} + C_{22} + C_{33} + 2\left(C_{12} + C_{13} + C_{23}\right)\right] > 0,\\
&\left(C_{11} + C_{22} - 2C_{12}\right) > 0,\\
&\left(C_{11} + C_{33} - 2C_{13}\right) > 0,\\
&\left(C_{22} + C_{33} - 2C_{23}\right) > 0.
\end{aligned} \tag{3}$$

Based on the above formulas, one can get the mechanical properties of $AFB_1$ under different pressures. From Fig. 3a, it can be seen the elastic modulus present rising trend on the whole, but show a descent trend under 15 and 20 GPa for $C_{66}$. Another descent point is 40 GPa. Thus, the structure of $AFB_1$ is not stable under these pressures. In fact, the value of $C_{11} + C_{22} - 2C_{12}$ is about −4.6 GPa, while $C_{22} + C_{33} - 2C_{23}$ equals approximately −28.8 GPa for the elastic modulus of $AFB_1$ under 0 GPa. One can find that pressure can easily change the structure of this organic toxin. However, the transformation of structure is a complex process unquestionably. Furthermore, we plan to make a prediction about structures of this toxin under different pressures. Based on the above elastic modulus, one can get bulk modulus $B$ and shear modulus $G$ of $AFB_1$; Here

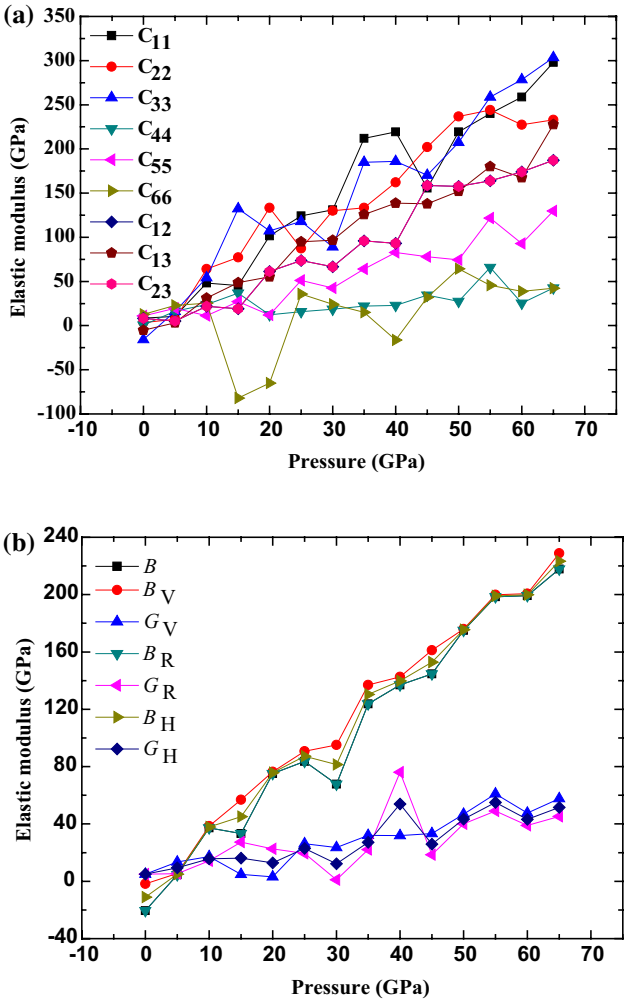


**Fig. 3** **a** Calculated elastic constants of $AFB_1$ under different pressures. **b** Variation of bulk modulus $B$ and shear modulus $G$ under different pressures

$$\begin{aligned}
B_{\mathrm{v}} &= (1/9)\left[C_{11} + C_{22} + C_{33} + 2\left(C_{12} + C_{13} + C_{23}\right)\right],\\
G_{\mathrm{v}} &= (1/15)\left[C_{11} + C_{22} + C_{33} + 3\left(C_{44} + C_{55} + C_{66}\right) - \left(C_{12} + C_{13} + C_{23}\right)\right],\\
B_{\mathrm{R}} &= \Delta\left[C_{11}\left(C_{22} + C_{33-}2C_{23}\right) + C_{22}\left(C_{33-}2C_{13}\right) - 2C_{33}C_{12} + C_{12}\left(2C_{23} - C_{12}\right) + C_{13}\left(2C_{12} - C_{13}\right) + C_{23}\left(2C_{13-}C_{23}\right)\right]^{-1},\\
G_{\mathrm{R}} &= 15\left\{4\left[C_{11}\left(C_{22} + C_{33} + C_{23}\right) + C_{22}\left(C_{33} + C_{13}\right) + C_{33}C_{12} - C_{12}\left(C_{12} + C_{23}\right) - C_{13}\left(C_{12} + C_{13}\right) - C_{23}\left(C_{13} + C_{23}\right)\right]/\right.\\
&\quad \left.\Delta + 3\left[\left(1/C_{44}\right) + \left(1/C_{55}\right) + \left(1/C_{66}\right)\right]\right\}^{-1},\\
\Delta &= C_{13}\left(C_{12}C_{23} - C_{13}C_{22}\right) + C_{23}\left(C_{12}C_{13} - C_{23}C_{11}\right) + C_{33}\left(C_{11}C_{22} - {C_{12}}^2\right).
\end{aligned} \tag{4}$$

In the above formulas, subscript V denotes the Voigt bound, R denotes the Reuss bound, and H denotes the Hill average. The Voigt bound calculated by the average polycrystalline moduli based on an assumption of uniform strain throughout a polycrystal and is the upper limit of the actual effective moduli. The Reuss bound calculated by assuming a uniform stress and is the lower limit of the actual effective moduli. The arithmetic average of Voigt and Reuss bounds is termed as the Voigt–Reuss–Hill approximations. The variation of bulk modulus $B$ and shear modulus $G$ with pressure is shown in Fig. 3b.

### 3.3 Optical properties

Considering the most common method on destroying the structure of organic substances using ultraviolet irradiation, it is necessary to have a detail investigation on the optical properties of $AFB_1$. This can offer useful assistance on reducing the toxicity using optical technology. The optical properties of the complex dielectric function are $\varepsilon(\omega) = \varepsilon_1(\omega) + i\varepsilon_2(\omega)$, where $\varepsilon_1(\omega)$ and $\varepsilon_2(\omega)$ represent the real part and the imaginary part of dielectric function, respectively. In general, $\varepsilon_2(\omega)$, resulting from direct interband transition, can be obtained from Fermi's golden rule:

$$\varepsilon_2(\omega) = \frac{2e^2\pi}{\Omega\varepsilon_0} \sum \left|\psi_k^c|\mathbf{u}\cdot\mathbf{r}|\psi_k^v\right|^2 \delta(E_k^c - E_k^v - E), \tag{5}$$

where $\omega$ denotes the frequency of the electromagnetic radiation in energy unit. $\Omega$ represents the cell volume and $\varepsilon_0$ is the dielectric constant in free space. $c$ and $v$ indicate the conduction and valence band states, respectively. In addition, $\mathbf{u}$ and $\mathbf{r}$ denote the vector defining the polarization of the incident electric field and the position vector, respectively. The real part of the dielectric function $\varepsilon_1(\omega)$ can be evaluated with its imaginary part $\varepsilon_2(\omega)$ using the Kramers–Kronig relation as follows [32]:

$$\varepsilon_1(\omega) = \frac{1}{\pi} P \int_{-\infty}^{+\infty} \frac{\varepsilon_2(\omega')}{\omega' - \omega} \mathrm{d}\omega', \tag{6}$$

where $P$ is the principal value of the integral. Other optical properties such as absorption coefficient $\alpha(\omega)$ and energy loss spectrum $L(\omega)$ can be expressed in terms of $\varepsilon_1(\omega)$ and $\varepsilon_2(\omega)$ as follows [33]:

$$\alpha(\omega) = \sqrt{2}\omega \left[\sqrt{\varepsilon_1^2(\omega) + \varepsilon_2^2(\omega)} - \varepsilon_1(\omega)\right]^{1/2}, \tag{7}$$

$$L(\omega) = \varepsilon_2(\omega) / \left[\varepsilon_1^2(\omega) + \varepsilon_2^2(\omega)\right]. \tag{8}$$

Figure 4 gives the results of the real and imaginary part of the dielectric function of aflatoxin $B_1$ under different polarizations. The dielectric peaks of $\varepsilon_2(\omega)$ of the dielectric function are related to the real transitions between occupied and unoccupied electronic states. From Fig. 4b, one can see that the dielectric function is in accordance with the Lorentz model, which is described as follows:

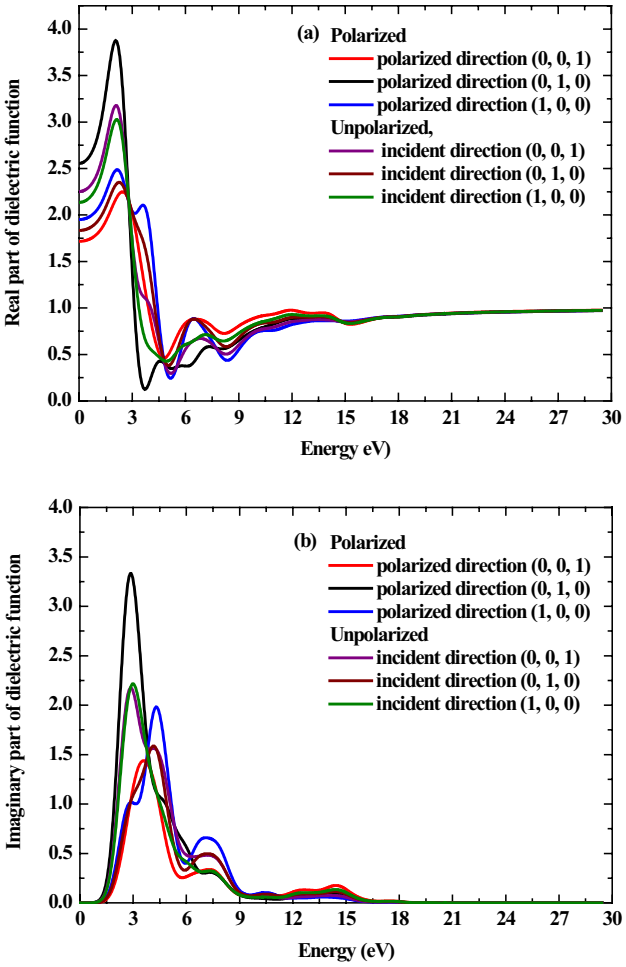


**Fig. 4** Real ($\varepsilon_1(\omega)$) and imaginary ($\varepsilon_2(\omega)$) part of dielectric function of $AFB_1$ for various conditions under 0 GPa

$$\varepsilon(\omega) = \varepsilon_1(\omega) + i\varepsilon_2(\omega) = 1 + \frac{\omega_P^2(\omega_O^2 - \omega^2)}{(\omega_O^2 - \omega^2)^2 - \omega/\tau^2} + i\frac{\omega_P^2\omega/\tau}{(\omega_O^2 - \omega^2) + (\omega/\tau)^2}, \tag{9}$$

where $\omega_O$ is the oscillator frequency. Lorentz dispersion theory is based on the damped harmonic oscillator approximation. On the other hand, the peak values of real (3.87) and imaginary (3.33) dielectric function for (0, 1, 0) direction under polarized condition are highest compared with other conditions. The dielectric function also indicates that this toxin presents well-insulating properties under 0 GPa. The optical absorption spectrum represents the fraction of energy that loses in passing through materials, and is directly related

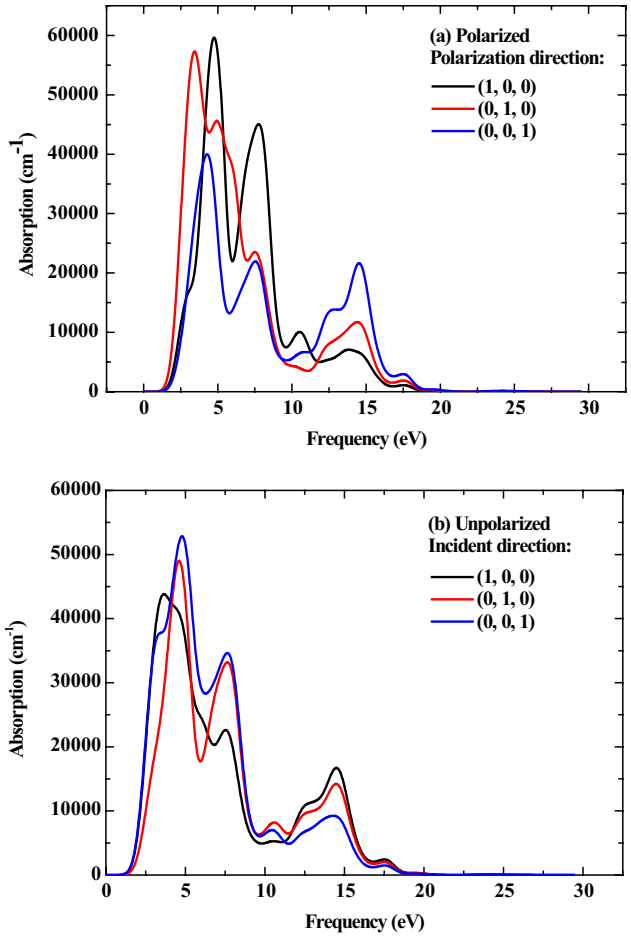


**Fig. 5** Absorption coefficient of $AFB_1$ with various frequencies under different polarization and incident directions

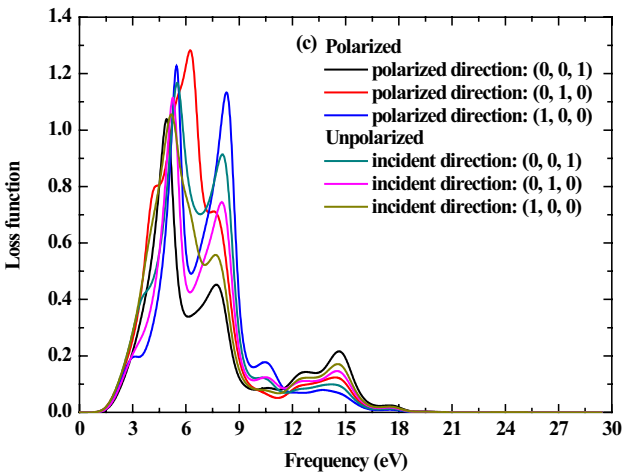


**Fig. 6** Energy loss function of $AFB_1$ with various different polarized and incident directions under polarized and unpolarized conditions

to the imaginary part of refractive index. The absorption coefficient over a wide range of frequencies, from the infrared to the ultraviolet regimes, is illustrated in Fig. 5, including polarized and unpolarized conditions. Through comparison, one can find that the absorption coefficient under polarization is larger than that under unpolarized conditions overall. The absorption behaviors are distinct for different polarization and incident directions. For the polarization direction (1, 0, 0), the absorption coefficient of infrared spectrum is highest, while (0, 0, 1) direction presents an excellent absorption of ultraviolet spectrum. Inversely, the absorption coefficient of infrared spectrum is highest for the incident direction corresponding to (0, 0, 1), while (1, 0, 0) incident direction exhibits a strong absorption for ultraviolet spectrum. Finally, the energy loss function is an important optical parameter, which describes the energy loss of electrons fast traversing in materials. The peaks of $L(\omega)$ characterize the plasma resonance and their peak positions correspond to the relevant plasma frequencies. The calculated energy loss function of $AFB_1$ under various pressures is illustrated in Fig. 6. One can find that the peak value along (0, 1, 0) polarized direction is highest at about 6.27 eV among different polarized and incident directions, meaning the energy loss of red light. On the other hand, the energy loss of ultraviolet becomes highest along the polarized direction (0, 0, 1). This is consist with the previous conclusion about absorption coefficients. Through the analysis of optical properties of $AFB_1$ under different conditions, one can find the absorption coefficient, dielectric function, and energy loss function of light are susceptible to the polarized and incident directions. These conclusions can offer important help on eliminating toxicity of $AFB_1$ using optical technologies.

## 4 Conclusions

The present study demonstrates basic structural, infrared spectrum, mechanical, and optical properties of aflatoxin under optimal pressure. The Mulliken charge distribution calculation explains detailed understanding of structural difference among four basic types of aflatoxins. The elastic constants and mechanical properties of $AFB_1$ calculated using first-principle calculations. In addition, it can be confirmed that pressure can easily change the structure of this organic toxin, since the values of $C_{11} + C_{22} - 2C_{12}$ and $C_{22} + C_{33} - 2C_{23}$ are negative for the elastic modulus of $AFB_1$ under 0 GPa. The real ($\varepsilon_1(\omega)$) and imaginary ($\varepsilon_2(\omega)$) parts of the dielectric function, the absorption coefficient $\alpha(\omega)$, and energy loss spectrum $L(\omega)$ are determined under different polarized and incident directions. A very important phenomenon is that these parameters of $AFB_1$ are anisotropic under different conditions. For the polarization direction (1, 0, 0), the absorption coefficient of infrared spectrum is highest, while (0, 0, 1) direction presents an

excellent absorption of unltraviolet spectrum. Inversely, the absorption coefficient of infrared spectrum is highest for the incident direction corresponding to (0, 0, 1), while (1, 0, 0) incident direction exhibits a strong absorption for unltraviolet spectrum. For the energy loss function of $AFB_1$, the value along (0, 1, 0) polarized direction is highest among different polarized and incident directions, meaning the energy loss of red light, while the energy loss of ultraviolet becomes highest along the polarized direction (0, 0, 1). Based on the results, we conclude, detoxification of $AFB_1$ using optical technologies is an economical and non-laborites method. Furthermore, biological experiment combined with pressure technology should be conducted to have a further study on the pressure-dependent detoxification of aflatoxins.

**Acknowledgements** The authors would like to thank the support by Special Program of Theoretical physics of National Natural Science Foundation of China under Grant nos. 11647124, 11647030 and 1404094, the Doctoral Fund of Henan University of Technology under Grant no. 2016BS006, the Science and Technology Foundation of Henan province education department under Grant nos. 16A140006 and 17A140016, the Fundamental Research Funds for the Henan Provincial Colleges, and University of Technology under Grant nos. 2016QNJH12 and 2016JJSB091. We also thank the support by the research fund of Sichuan University of Science and Engineering under Grant nos. 2015RC41 and J2015RC44, the Education Department of Sichuan Province under Grant no. 17ZA0278, as well as the China Postdoctoral Science Foundation funded project under Grant no. 2017M623310XB.

## References

1. Davis ND, Diener UL, Eldridge DW (1966) Production of aflatoxins B1 and G1 by Aspergillus flavus in a semisynthetic medium. Appl Environ Microbiol 14(3):378–380
2. Wilson DM, Mubatanhema W, Jurjevic Z (2002) Biology and ecology of mycotoxigenic Aspergillus species as related to economic and health concerns. Adv Exp Med Biol 504:3–17
3. Egal S, Hounsa A, Gong YY, Turner PC, Wild CP, Hall AJ, Hell K, Cardwell KF (2005) Dietary exposure to aflatoxin from maize and groundnut in young children from Benin and Togo. West Africa Int J Food Microbiol 104:215–224
4. Yang ZY, Shim WB, Kim JH, Park SJ, Kang SJ, Nam BS, Chung DH (2004) Detection of aflatoxin-producing molds in Korean fermented foods and grains by multiplex PCR. J Food Prot 67:2622–2626
5. Dawlatana M, Coker RD, Nagler MJ, Wild CP, Hassan MS, Blunden G (2002) The occurrence of mycotoxins in key commodities in Bangladesh: surveillance results from 1993 to 1995. J Nat Toxins 11:379–386
6. Park JW, Kim EK, Kim YB (2004) Estimation of the daily exposure of Koreans to aflatoxin B1 through food consumption. Food Addit Contam 21:70–75
7. Park JW, Choi SY, Hwang HJ, Kim YB (2005) Fungal mycoflora and mycotoxins in Korean polished rice destined for humans. Int J Food Microbiol 103:305–314
8. Stoloff L, Trucksess MW (1981) Effect of boiling frying, and baking on recovery of aflatoxin from naturally contaminated corn grits or cornmeal. J Assoc Off Anal Chem 64:678–680
9. Cazzaniga D, Basilico JC, Gonzalez RJ, Torres RL, de Greef DM (2001) Mycotoxins inactivation by extrusion cooking of corn flour. Lett Appl Microbiol 33:144–147
10. Elias-Orozco R, Castellanos-Nava A, Gaytan-Martinez M, Figueroa-Cardenas JD, Loarca-Pina G (2002) Comparision of nixtamalization and extrusion processes for a reduction in aflatoxin content. Food Addit Contam 19:878–885
11. Dakovic A, Matijašević S, Rottinghaus GE, Ledoux DR, Butkeraitis P, Sekulic Z (2008) Aflatoxin $B_1$ adsorption by natural and copper modified montmorillonite. Colloids Surf B 66(1):20–25
12. Huertas-Pérez JF, Arroyo-Manzanares N, Hitzler D, Castro-Guerrero FG, Gámiz-Gracia L, García-Campaña AM (2018) Simple determination of aflatoxins in rice by ultra-high performance liquid chromatography coupled to chemical post-column derivatization and fluorescence detection. Food Chem 245:189–195
13. Golge O, Hepsag F, Kabak B (2016) Determination of aflatoxins in walnut sujuk and Turkish delight by HPLC-FLD method. Food Control 59:731–736
14. Martins LM, Sant'Ana AS, Fungaro MHP, Silva JJ, Nascimento MS, Frisvad JC, Taniwaki MH (2017) The biodiversity of *Aspergillus* section *Flavi* and aflatoxins in the Brazilian peanut production chain. Food Res Int 94:101–107
15. Adebo OA, Njobeh PB, Gbashi S, Nwinyi OC, Mavumengwana V (2017) Review on microbial degradation of aflatoxins. Crit Rev Food Sci 57(15):3208–3217
16. Park JW, Kim YB (2006) Effect of pressure cooking on aflatoxin B1 in rice. J Agric Food Chem 54:2431–2435
17. Patras A, Julakanti S, Yannam S, Bansode RR, Burns M, Vergne MJ (2017) Effect of UV irradiation on aflatoxin reduction: a cytotoxicity evaluation study using human hepatoma cell line. Mycotoxin Res 33(4):343–350
18. Shahin AA, Aziz NH (1997) Influence of gamma rays and sodium chloride on aflatoxin production by *Aspergillus flavus*. Microbios 90(364):163–175
19. Hanwell MD, Curtis DE, Lonie DC, Vandermeersch T, Zurek E, Hutchison GR (2012) Avogadro: an advanced semantic chemical editor, visualization, and analysis platform. J Cheminformatics 4(1):17
20. Frisch MJ, Trucks GW, Schlegel HB, Scuseria GE, Robb MA, Cheeseman JR, Scalmani G, Barone V, Mennucci B, Petersson GA, Nakatsuji H, Caricato M, Li X, Hratchian HP, Izmaylov AF, Bloino J, Zheng G, Sonnenberg JL, Hada M, Ehara M, Toyota K, Fukuda R, Hasegawa J, Ishida M, Nakajima T, Honda Y, Kitao O, Nakai H, Vreven T, Montgomery JA Jr, Peralta JE, Ogliaro F, Bearpark M, Heyd JJ, Brothers E, Kudin KN, Staroverov VN, Keith T, Kobayashi R, Normand J, Raghavachari K, Rendell A, Burant JC, Iyengar SS, Tomasi J, Cossi M, Rega N, Millam JM, Klene M, Knox JE, Cross JB, Bakken V, Adamo C, Jaramillo J, Gomperts R, Stratmann RE, Yazyev O, Austin AJ, Cammi R, Pomelli C, Ochterski JW, Martin RL, Morokuma K, Zakrzewski VG, Voth GA, Salvador P, Dannenberg JJ, Dapprich S, Daniels AD, Farkas O, Foresman JB, Ortiz JV, Cioslowski J, Fox DJ (2009) Gaussian 09, Inc, Wallingford
21. Payne MC, Teter MP, Allen DC, Arias TA, Joannopoulos JD (2008) Iterative minimization techniques for ab initio total-energy calculations: molecular dynamics and conjugate gradients. Rev Mod Phys 64:4(4):1045
22. Milman V, Winkler B, White JA, Packard CJ, Payne MC, Akhmatskaya EV, Nobes RH (2000) Electronic structure, properties, and phase stability of inorganic crystals: a pseudopotential plane-wave study. Int J Quantum Chem 77:895–910
23. Vanderbilt D (1990) Soft self-consistent pseudopotentials in a generalized eigenvalue formalism. Phys Rev B 41:7892–7895
24. Perdew JP, Burke K, Ernzerhof M (1996) Generalized gradient approximation made simple. Phys Rev Lett 77:3865–3868

25. Monkhorst HJ, Pack JD (1976) Special points for Brillouin-zone integrations. Phys Rev B 13:5188
26. Fischer TH, Almlof J (1992) General methods for geometry and wave function optimization. J Phys Chem 96:9768–9774
27. Pfrommer BG, Côté M, Louie SG, Cohen ML (1997) Relaxation of crystals with the Quasi-Newton method. J Comput Phys 131:233–240
28. Allen FH, Davies JE, Johnson OJ, Kennard O, Macrae CF, Mitchell EM, Smith GF, Watson DG (1991) The developments of version 3 and 4 of the Cambridge Database System. J Chem Inf Comput Sci 31:187–204
29. Karki BB, Ackland GJ, Grain J (1997) Elastic instabilities in crystals from ab initio stress-strain relations. J Phys Condens Matter 9:8579
30. Wei YK, Yu JX, Li ZG, Cheng Y,. Ji GF (2011) Elastic and thermodynamic properties of CaB6 under pressure from first principles. Physica B 406:4476–4482
31. Wallace DC (1972) Thermodynamics of crystals. Wiley, New York
32. Li YL, Fan WL, Sun HG, Cheng XF, Li P, Zhao X (2010) Structural, electronic, and optical properties of α, β, and γ-$TeO_2$. J Appl Phys 107:093506
33. Saha S, Sinha TP (2000) Electronic structure, chemical bonding, and optical properties of paraelectric $BaTiO_3$. Phys Rev B 62:8828–8834